Mühendislik Bilimleri ve Tasarım Dergisi
14(2), 233-253, 2026
e-ISSN: 1308-6693

Journal of Engineering Sciences and Design
DOI: 10.21923/jesd.1836755

Araştırma Makalesi

Research Article

THE EFFECT OF WAVE PARAMETERS ON AERODYNAMIC COEFFICIENTS DURING WING-IN-GROUND EFFECT FLIGHT

Mehmet BAKIRCI*

* Karabük University, TOBB Technical Sciences Vocational School Department of Electronics and Automation, Karabük, Türkiye

Keywords

Wavy ground, Lift, Drag, Wavelength, Wave Amplitude, Unsteady RANS.

Abstract

In this study, the ground effect, which affects the aerodynamic performance of aircraft flying near wavy ground was investigated with time-dependent 2D Unsteady RANS-based Computational Fluid Dynamics (CFD) analyses. Analyses were conducted using a NACA 4412 airfoil under various wave amplitudes, wavelengths, and angles of attack. In the analyses, the airfoil was held stationary, and a sinusoidal moving ground model was applied underneath to simulate the periodic wave effect. The variation of lift, drag, and moment coefficient (C_L, C_D, C_m) values according to different wave positions was determined. It was determined that the highest C_L occurred when approaching the wave crest and the lowest when approaching the trough. The effects of wave parameters, angles of attack, and proximity to the ground on the airfoil were analyzed. Results reveal that lift coefficient (CL) varies by 26.04 % over a wave period (from 0.962 to 1.250) for the most dynamic case (AOA=8°, h/c=0.4, λ/c=1, α/c=0.2). Maximum lift occurs at wave crests (CL=1.250), representing a 14.2% increase relative to time-averaged values, while minimum lift at wave troughs shows a 13% decrease. Ground clearance reduction from h/c=0.8 to h/c=0.4 amplifies fluctuations by 37%, while wavelength increase from λ/c=1 to λ/c=3 reduces variations by 58%.

YER ETKİSİ ALTINDA UÇUŞTA DALGA PARAMETRELERİNİN AERODİNAMİK KATSAYILAR ÜZERİNDE ETKİSİ

Anahtar Kelimeler

Dalgalı zemin, Kaldırma kuvveti, Sürükleme kuvveti, Dalga boyu, Dalga genliği, Kararsız RANS.

Öz

Bu çalışmada, dalgalı zemine yakın uçan uçakların aerodinamik performansını etkileyen zemin etkisi, zamana bağlı 2D Kararsız RANS tabanlı Hesaplamalı Akışkanlar Dinamiği (CFD) analizleri ile incelenmiştir. Analizler, çeşitli dalga genlikleri, dalga boyları ve hücum açıları altında NACA 4412 kanat profili kullanılarak gerçekleştirilmiştir. Analizlerde, kanat profili sabit tutulmuş ve periyodik dalga etkisini simüle etmek için altına sinüzoidal hareketli zemin modeli uygulanmıştır. Farklı dalga konumlarına göre kaldırma, sürtünme ve moment katsayısı (C_L, C_D, C_m) değerlerinin değişimi belirlenmiştir. En yüksek C_L 'nin dalga tepesine yaklaşırken, en düşük C_L 'nin ise dalga çukuruna yaklaşırken meydana geldiği belirlenmiştir. Dalga parametrelerinin, hücum açılarının ve zemine yakınlığın kanat profili üzerindeki etkileri analiz edilmiştir. Sonuçlar, en dinamik durumda (AOA=8°, h/c=0,4, λ/c=1, α/c=0,2) kaldırma katsayısının (CL) dalga periyodu boyunca %26,04 oranında değiştiğini (0,962'den 1,250'ye) ortaya koymaktadır. En yüksek kaldırma kuvveti dalga tepelerinde (CL=1,250) meydana gelir ve bu da zaman ortalamalı değerlere göre %14,2'lik bir artışı temsil ederken, dalga çukurlarında minimum kaldırma kuvveti %13'lük bir azalma göstermektedir. Yerden yüksekliğin h/c=0,8'den h/c=0,4'e düşmesi dalgalanmaları %37 oranında artırırken, dalga boyunun λ/c=1'den λ/c=3'e artması varyasyonları %58 oranında azaltmaktadır.

Alıntı / Cite

Bakırcı, M., (2026). The Effect of Wave Parameters on Aerodynamic Coefficients During Wing-In-Ground Effect Flight, Journal of Engineering Sciences and Design, 14(2), 233-253.

Yazar Kimliği / Author ID

M. Bakırcı, 0000-0002-1061-698X

Makale Süreci / Article Process

Başvuru Tarihi / Submission Date	05.12.2025
Revizyon Tarihi / Revision Date	11.03.2026
Kabul Tarihi / Accepted Date	05.04.2026
Yayım Tarihi / Published Date	30.06.2026

* İlgili yazar / Corresponding author: mehmetbakirci@karabuk.edu.tr, +90 0532 663 9124

THE EFFECT OF WAVE PARAMETERS ON AERODYNAMIC COEFFICIENTS DURING WING-IN-GROUND EFFECT FLIGHT

Mehmet Bakırcı†
Karabük University, TOBB Technical Sciences Vocational School, Department of Electronics and Automation, Karabük, Türkiye

Highlights

- The study contributes to the literature on the multi-parameter, time-dependent interaction of aerodynamic loads under the influence of wavy ground.
- The most important finding is that maximum lift occurs at the wave crest, while maximum drag occurs at the wave trough.
- The findings can be used in the design optimization and control algorithm development of ground effect vehicles.

Graphical Abstract

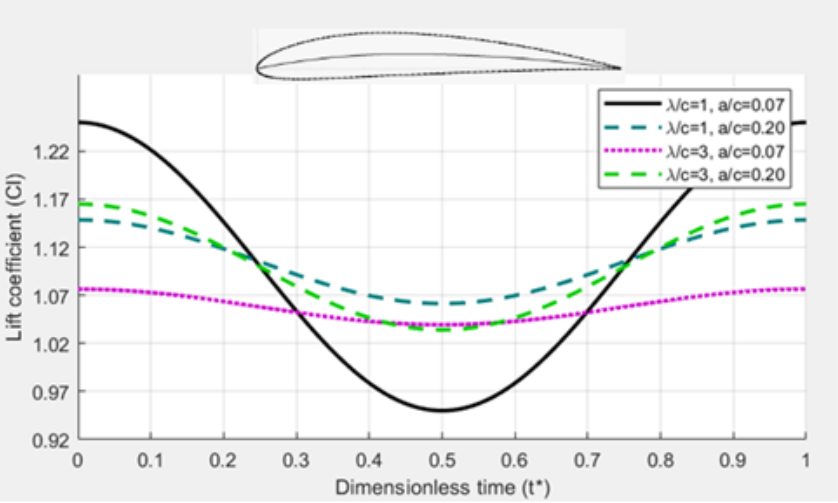

Graphical Abstract. Variation of C_L value depending on wave parameters

Purpose and Scope

The primary objective of the study is to investigate in detail the variation of lift (C_L), drag (C_D), and moment (C_m) coefficients on an airfoil exposed to ground effect under wavy ground conditions with respect to time and wave location. The effects of wave crests, troughs, and intermediate locations, as well as angle of attack (AOA), surface height (h/c), wave amplitude (α/c), and wavelength (λ/c) on aerodynamic loads are evaluated. The study aims to better understand the stability problems encountered in ground effect systems such as ekranoplans, seaplanes, airfish-8 vehicles, unmanned aerial vehicles, and the potentially future Aerotrain.

Methodology

The study was conducted using time-dependent Unsteady RANS-based CFD analysis. The ground was modeled as rigid, and the wavy surface was manipulated using a sliding mesh method to achieve realistic wave-wing interactions. The maximum, minimum, and fluctuation characteristics of the C_L, C_D, and C_m coefficients were analyzed by systematically varying the angle of attack (0° and 8°), ground clearance, wave amplitude, and wavelength parameters. The study goes beyond single-parameter analysis and presents a holistic approach that explores the multi-parameter and periodic nature of aerodynamic loads.

Findings

(1) Wavelength increase from λ/c=1 to λ/c=3 reduces lift fluctuations by 58% (ΔCL from 0.083 to 0.035),
(2) Wave amplitude increases from α/c=0.07 to α/c=0.2 amplifies drag variations by 50%,
(3) Angle of attack increases from 0° to 8° intensifies all fluctuations by over 250%.

Originality

The study is an original study that examines the temporal and periodic effects of ground effect on aerodynamic loads under wavy ground, including the C_L, C_D, and C_m coefficients, by considering all key geometric and flow parameters. Unlike studies in the literature that typically focus on a single parameter, this research clearly demonstrates the role of multi-parameter interactions on stability. The findings offer significant contributions to researchers and engineering practices in the development of design optimization and control algorithms for ekranoplans, seaplanes, UAVs, Airfish-8, and similar ground-effect systems.

† İlgili yazar / Corresponding author: mehmetbakirci@karabuk.edu.tr, +90 0532 663 9124

1. Introduction

Ground-effect vehicles (GEVs) such as Ekranoplan and Airfish-8 achieve significantly higher lift-to-drag ratios compared to conventional aircraft by leveraging the aerodynamic interaction between the wing and the ground surface, thus enabling high-speed maritime transport with exceptional fuel efficiency (Rozhdestvensky, 2006). By compressing high-pressure air between the wing and the water surface, these vehicles bridge the gap between the speed of aircraft and the payload capacity of conventional ships, offering transformative potential for both commercial and military applications. However, widespread adoption of GEV technology is severely hampered by aerodynamic instability caused by surface irregularities, primarily ocean waves. Unlike a flat surface, a wavy surface constantly changes the instantaneous ground clearance as the vehicle passes wave crests and troughs, redirecting the direction of the incoming flow. This periodic change leads to time-dependent fluctuations in lift, drag, and pitching moment coefficients, exacerbating phenomena such as flow separation, eddy spill, stall, and reconnection. This creates significant challenges in terms of vehicle stability and control (Hu and Ma, 2020; Liu et al., 2021; Liang, Zong and Zou, 2013). Even negative lift can occur under high wave amplitude and low angle of attack conditions, leading to critical safety risks (Liu, 2021). To develop effective stability and control strategies for GEV and wing-to-ground impact (WIG) systems operating in realistic sea conditions, a comprehensive and quantitative understanding of these periodic aerodynamic loads under parametrically modified wave conditions is essential.

This study is guided by three main research streams. The first stream concerns aerodynamic performance under flat ground conditions and has been comprehensively addressed through theoretical, experimental, and computational studies. Wind tunnel experiments and CFD (Computational Fluid Dynamics) analyses have revealed the fundamental mechanisms of ground effect—Venturi-induced flow compression, increased bottom surface pressure, and decreased induced drag—over a wide range of airfoil geometries, length/chord ratios, ground clearance (h/c = 0.05–1.0), and angle of attack (0°–18°) (Ahmed, 2006; Ahmed, 2007; Zaheer et al., 2019; Firooz and Gadami, 2006; Tofa et al., 2014). These studies validated the SST k-ω turbulence model as the most reliable RANS approach for ground effect flows, forming the methodological basis of the present research. The second approach encompasses undulating ground conditions where sliding mesh techniques are used to simulate sinusoidal wave motion. Current studies have investigated the variation of aerodynamic coefficients for limited parameter combinations: Hu and Ma (2020) studied a wide range of angles of attack in a constant wave geometry; Liu et al. (2021) studied variable wave amplitudes only under the condition AOA = 0°; and Liang, Zong, and Zou (2013) addressed nonlinear lift theory for two-dimensional wave interactions. The third approach focuses on control system requirements for GEV and WIG vehicles, revealing that real-time aerodynamic load data constitutes critical input for flight control design with automated stabilization algorithms (Nebylov and Synyavskiy, 2013; Matdaud et al., 2019; Su et al., 2023). A consistent gap is evident across the three streams: no study has systematically and multi-parametrically investigated the combined effects of AOA, ground clearance, wave amplitude, and wavelength on time-dependent aerodynamic loads. Systematic analysis of the variation of aerodynamic coefficients (CL, CD) with angle of attack is similarly applied in UAV wing profile optimization studies [Celik, 2025].

This study presents a comprehensive parametric CFD investigation of aerodynamic coefficient fluctuations during flight on a sinusoidal wavy ground for the NACA 4412 airfoil to fill the aforementioned gap. Sixteen combinations of systematic parameters were investigated: angle of attack (AOA = 0° and 8°), dimensionless ground clearance (h/c = 0.4 and 0.8), wave amplitude (α/c = 0.07 and 0.2), and wavelength (λ/c = 1 and 3). Two-dimensional Unsteady RANS (URANS) simulations were performed using the SST k-ω turbulence model and sliding mesh technique, following the established methodology of Hu and Ma (2020) and Liu et al. (2021); validation was performed with experimental data from Ahmed (2006) on a flat ground.

2. Methodology

This study adopted a detailed methodology based on CFD analysis to comprehensively investigate the aerodynamic performance of aircraft moving under the influence of wavy ground and to determine the aerodynamic design parameters such as AOA and ground clearance for optimum flight. In the analyses, the airfoil was positioned at a specific distance from the water surface. To accurately analyze the aerodynamic effects of wave motion, various angles of attack, velocities, and airfoil heights above the ground were parametrically investigated. The wave surface was generated using a sinusoidal wave model, with wavelength (λ) and wave amplitude (α) defined as variable parameters. This systematically investigated the effects of wave geometry on the lift (C_L), drag (C_D), and moment (C_m) coefficients of the airfoil.

In this study, a two-dimensional transient CFD analysis was performed to investigate the effect of wavy ground on the NACA4412 airfoil. The computational domain shown in Figure 1 was divided into two distinct regions, upper

and lower. In the upper region, the airfoil was held fixed, while the lower region simulated moving ground containing sinusoidal waves. In the study, analyses were conducted for 16 different cases (Table 1) for different dimensionless wave amplitudes (α/c; 0.07 and 0.2) and wavelengths (λ/c; 1 and 3) using a speed of 30.8 m/s, a chord length of c=0.15 m, and AOA values are 0° and 8°.

Table 1. 16 cases where CFD analyses were performed

Cases	AOA	h/c	α/c	λ/c	Cases	AOA	h/c	α/c	λ/c
1	0°	0.4	0.07	1	9	8°	0.4	0.07	1
2	0°	0.4	0.2	1	10	8°	0.4	0.2	1
3	0°	0.4	0.07	3	11	8°	0.4	0.07	3
4	0°	0.4	0.2	3	12	8°	0.4	0.2	3
5	0°	0.8	0.07	1	13	8°	0.8	0.07	1
6	0°	0.8	0.2	1	14	8°	0.8	0.2	1
7	0°	0.8	0.07	3	15	8°	0.8	0.07	3
8	0°	0.8	0.2	3	16	8°	0.8	0.2	3

The four different wave forms; 1) λ/c=1, α/c=0.07, 2) λ/c=3, α/c= 0.07, 3) λ/c=1, α/c=0.2, 4) λ/c=3, α/c=0.2 are shown in Figure 1.

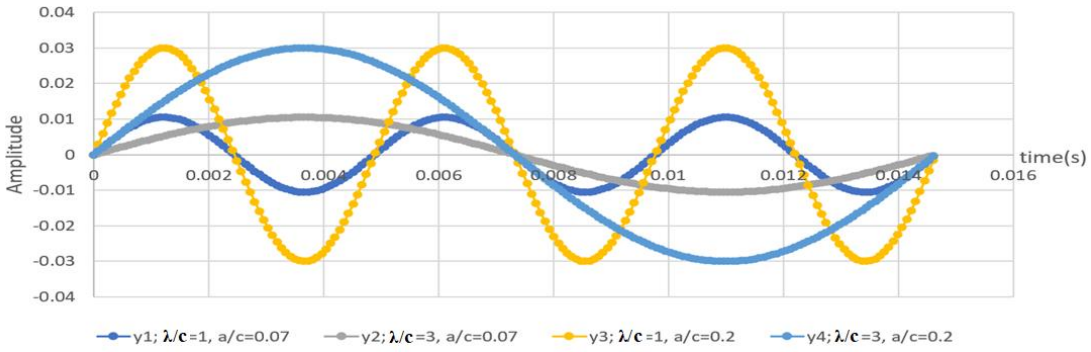

Figure 1. Four different waveforms (amplitudes are in meters)

The CFD computational domain was divided into two main parts: the upper and lower parts. The upper part contains the airfoil and the surrounding air environment. In this region, a velocity inlet boundary was defined to determine the initial conditions for the flow, and a pressure outlet boundary was defined, through which the flow can exit freely. In the upper region, farfield boundaries were used for the upper boundaries of the computational domain. The lower region represents the water region where wave motion would be generated. An interface was defined between the upper and lower regions to accurately simulate the airfoil's interaction with waves. The velocity input boundary of the lower region was determined to be equal to the wave speed (Figure 2).

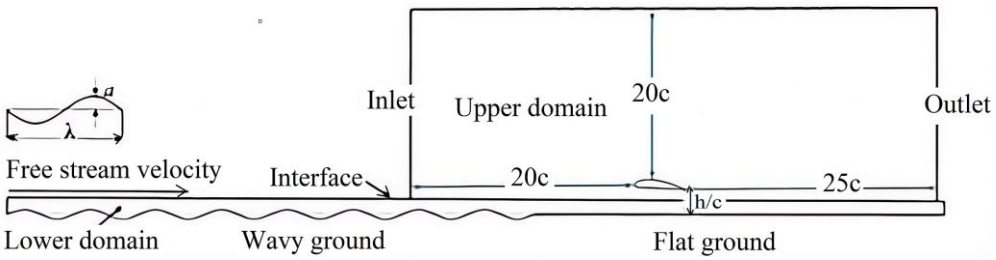

Figure 2. Computational Fluid domain geometry and boundary conditions [Hu & Ma, 2020]

A high-resolution triangular mesh structure was used around the airfoil during the computational mesh generation process, as shown in Figure 2. Quadrilateral meshes are often preferred for their potential to provide more stable and accurate solutions in certain flow problems. However, in this study, due to the combined consideration of both the airfoil geometry and the waveform, the mesh geometry resulted in a rather complex one. This made it difficult to create a regular and high-quality quadrilateral mesh, and a low-quality mesh structure

could lead to convergence problems, loss of accuracy, and increased computational time. Furthermore, even if all these challenges were overcome, much higher computational capacity would be required. For these reasons, a mesh structure consisting of triangular elements was preferred to obtain a higher-quality mesh. Furthermore, a 10-layer inflation was applied around the airfoil to accurately analyze the boundary layer flow on the airfoil surface(Figure 3).

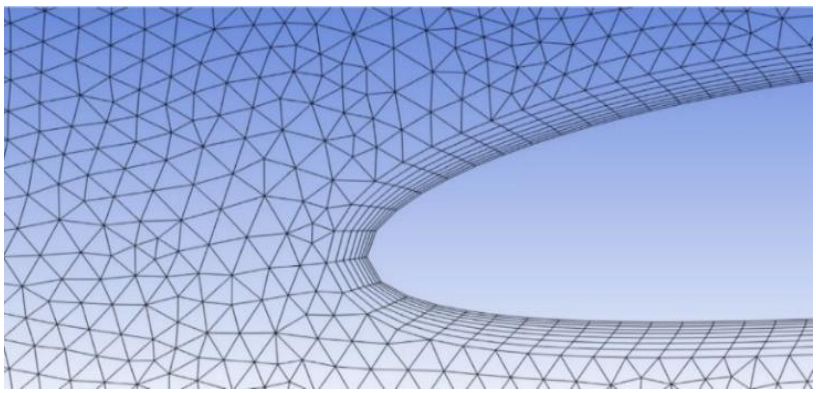

Figure 3. Triangular mesh structure and mesh details created around the wing profile

Mesh independence studies were conducted by testing meshes with different cell numbers to evaluate the solution sensitivity and ensure mesh independence. The SST k−ω model which has been used frequently in the Literature [Qu, Q., Wang, W., Liu, P., and Agarwal, RK (2015), Kaya (2025)] was preferred because it provides fast and reliable solutions for turbulence modeling. As required by this model, the initial cell height (Y+) on the airfoil and wavy ground surface was set to Y+≈1. Achieving temporal convergence is crucial for unsteady CFD analyses. Therefore, the time step (Δt) was determined so that the Courant-Friedrichs-Lewy (CFL) number CFL≤1. The optimum Δt value was selected using the equation Δt=(λ/V) ×CFL, depending on the wave period (λ/V). At each time step, iterations were continued until the residual errors for the momentum and turbulence equations were less than 10−6, thus achieving solution convergence. These rigorous convergence criteria ensured that the temporal variations of the obtained aerodynamic coefficients were accurate and reliable. CFD simulations were carried out at a Reynolds number of 314 285 under Ahmed's reference experimental conditions. The main objective was to accurately estimate C_L and C_D at 0° and 8° AOA using different mesh configurations and turbulence models.

2.1. Mesh Validation and Grid Accuracy Review

Five different meshes (Grid A, B, C, D and Fine Grid) were evaluated for lift and drag force coefficient accuracy, wall convergence (Y^+), CFL stability and computational efficiency:

Grid A: The coarsest mesh (Δx_{max}=7.0e -4 m) was used with the SST k-ω model with Y^+=2.8 and CFL=7. C_L=0.305 (18.2% error) was obtained compared to the experimental C_L (0.373) and C_D = 0.0158 (97.5% error) was obtained compared to the experimental C_D (0.0080).

Grid B: A more refined grid (Δx_{max}=5.0e -4 m). With y^+ =2.8, CFL=1.38, and the SST k-ω model, it yielded C_L=0.339 (9.1% error) and C_D = 0.0158 (97.5% error). Despite the high drag error, it was selected for subsequent analyses because it offered the best balance of lift accuracy and numerical stability.

Grid C1: This fine mesh (Δx ≈ 3.5e -4 m) used with the SAS turbulence model has high errors such as 39.4% in the C_L estimation and 86.3% in the C_D estimation. The y^+ and CFL values are out of control, and it is seen that the SAS model does not capture the lift feature sufficiently.

Grid C2: The SST k-ω model is a very fine mesh (Δx ≈ 3.5e -4 m), with y^+ = 1.34 and CFL=1.36. The C_L error was found to be 9.7% and C_D was found to be 87.5%. The drag prediction accuracy is similar to Grid B, but the computational cost is higher.

Grid D: This is the mesh with the highest resolution (Δx ≈ 2.5e -4 m), using the SST k-ω model with y^+ = 0.96 and CFL=1.11. The lowest drag error (C_D=0.0142) with 77.5% error was obtained. However, this mesh did not provide a marginal gain compared to Grid B, despite the increased computational cost.

Convergence criteria were applied meticulously, time step sensitivity analysis was performed and generally high

accuracy results were obtained (Table 2).

Table 2. Grid independence study

CASE	AOA (°)	C_L (EXP.)	C_L (CFD)	C_L Error (%)	C_D (EXP.)	C_D (CFD)	C_D Error (%)	Y^+	CFL	Turbulence Model
GRID A	0	0.373	0.305	18.2%	0.0080	0.0158	97.5%	2.8	7.00	SST k-ω
GRID B	**0**	**0.373**	**0.339**	**9.1%**	**0.0080**	**0.0158**	**97.5%**	**2.8**	**1.38**	**SST k-ω**
GRID C1	0	0.373	0.226	39.4%	0.0080	0.0149	86.3%	—	—	SAS
GRID C2	0	0.373	0.337	9.7%	0.0080	0.0150	87.5%	1.34	1.36	SST k-ω
GRID D	0	0.373	0.335	10%	0.0080	0.0142	77.5%	0.96	1.11	SST k-ω
GRID B	**8**	**1.291**	**1.265**	**2.0%**	**0.0157**	**0.0185**	**17.8%**	**2.8**	**1.38**	**SST k-ω**

Simulations performed with Grid B at an AOA of 8° yielded C_L =1.265 with a 2% error compared to the experimental C_L (1.291). The predicted C_D (0.0185) contained a 17.8% error compared to the experimental C_D (0.0157), which was considered acceptable, reflecting the sensitivity of the drag estimates to the turbulence model and mesh resolution. The SST k-ω turbulence model provided superior results to the SAS model with reliable prediction performance in the boundary layer and separation regions. The relatively high error rates in the drag predictions should be evaluated within the inherent limitations of CFD, and the results should be considered valid and reliable. This validated configuration (Grid B + SST k-ω) provides a solid basis for advanced unsteady aerodynamic analyses under the ground influence. The mesh independence study was carried out by comparing mesh structures at different resolutions (coarse, medium, fine) and it was confirmed that the results are independent of mesh resolution (Kaya, 2025).

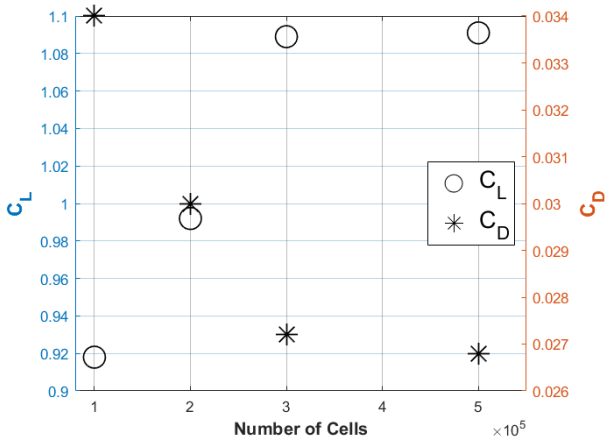

Figure 4. Mesh independence study (AOA=8°, h/c=0.4)

Mesh convergence study (Figure 4) showing variation of lift and drag coefficient errors with cell count at AOA=8°, h/c=0.4. Grid B (≈300,000 cells) was selected based on convergence threshold and computational efficiency. Further refinement yields marginal improvement at 3-5× computational cost.

Figure 5 shows the time-dependent variation of the lift coefficient for a 0° AOA on wavy terrain, obtained during the CFD iteration process. It is observed that the lift coefficient exhibits a periodic behavior under the influence of sinusoidal waves. The average lift coefficient was calculated as 0.36815, demonstrating the effect of wavy terrain on wing performance.

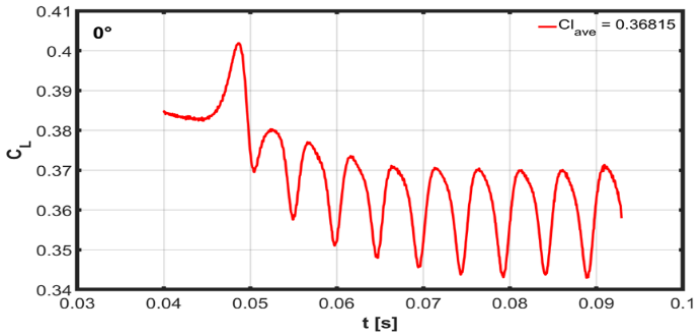

Figure 5. Periodic variation of lift coefficient with time at 0° AOA

For validation purposes, the C_L and C_D values obtained as a result of CFD analysis are compared with the Ahmed experimental study [Ahmed, 2006] results given in the literature in Table 3.

Table 3. Validation with Ahmed-2006 experiment results [Ahmed,2006].

	C_L				C_D		
AOA	**h/c**	**Present study**	**Exp. (Ahmed-2006)**	**AOA**	**h/c**	**Present study**	**Exp. (Ahmed-2006)**
0°	0.4	0.368	0.448	0	0.4	0.016	0.008
0°	0.8	0.391	0.460	0	0.8	0.017	0.008
8°	0.4	1.091	1.275	8	0.4	0.027	0.015
8°	0.8	1.086	1.274	8	0.8	0.028	0.014

This study employs two-dimensional URANS analysis to investigate the parametric effects of wavy ground on airfoil aerodynamics. While 2D analysis has been extensively validated in ground effect literature (Ahmed et al., 2007; Qu et al., 2014; Hu & Ma, 2020; Liu et al., 2021) and successfully captures the fundamental flow physics—including pressure distribution variations, ground clearance effects, and time-dependent load fluctuations—it does not account for three-dimensional effects such as wingtip vortices, spanwise flow, and finite aspect ratio influences.

2.2. Wavy Ground Validation and Literature Consistency

Qualitative trend consistency with wavy ground literature. Although experimental data are unavailable, independent numerical studies by multiple research groups provide qualitative benchmarks. four major wavy ground investigations (Qu et al. (2014), Hu and Ma (2020), and Liu et al. (2021), Liang et al. (2013)), despite using different parameter values and numerical approaches, report consistent physical trends: (a) maximum lift at wave crests, minimum at troughs; (b) longer wavelengths reduce fluctuation amplitudes; (c) higher angles of attack amplify fluctuations; (d) reduced ground clearance intensifies both mean loads and fluctuations. The present results exhibit good qualitative alignment with these trends, suggesting that the underlying flow physics is correctly represented.

3. CFD Results

As a result of the CFD analyses, contours such as velocity, velocity streamlines, pressure, and turbulence kinetic energy, along with pressure coefficient (CP) graphs, were obtained. The changes in the flow field were examined while the airfoil was positioned at different locations of the wave. The lift, drag, and moment values acting on the airfoil were analyzed for each wave position. Accordingly, C_L, C_D, and C_m values were determined when the airfoil

was located at the wave crest, trough, and during the crest–trough and trough–crest transitions. Using these obtained values, graphs were plotted to illustrate how C_L, C_D, and C_m vary with the different positions of the wave, i.e., as a function of time.

3.1. Pressure distributions varying according to different positions of the wave

The velocity streamlines obtained from the CFD analysis are given in Figure 6-9. The streamline contours show the velocity distributions obtained at different positions of the NACA 4412 airfoil on wavy ground. Each figure reveals how the flow behavior around the airfoil changes at different positions of the wave. The airfoil-wave location was determined using the dimensionless time defined as T=λ/V and t*=t/T, where T is the wave period, V is the airfoil speed (flow velocity = wave velocity), and t is the actual time (s).

The airfoil's leading edge is at the wave crest position. Due to the slope of the wavy surface, the flow dynamics change, and the angle of incidence of the flow over the wing and the resulting C_L, C_D, and C_m values are affected by this (t*=0) . The contour obtained for Case 12 (8°, h/c=0.4, λ=3c, α=0.2c) at t*=0 is shown in Figure 6.

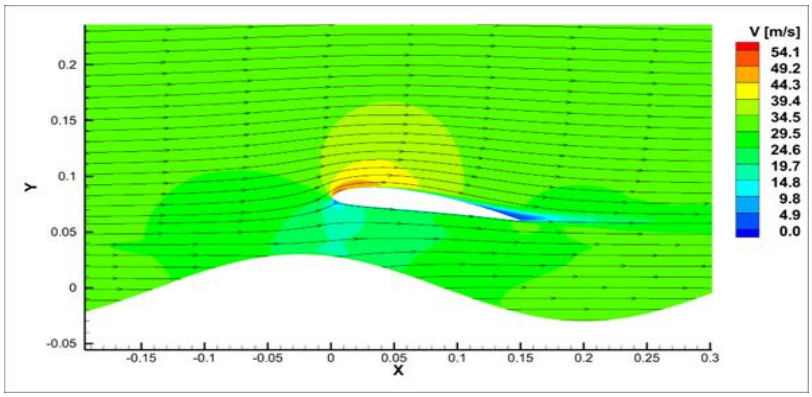

Figure 6. Streamline velocity contour**,** airfoil's leading edge at wave crest position (t*=0)

In this case, where the airfoil's leading edge is positioned above the wave crest, the ground effect is most intense. This is the position where maximum lift occurs. The wave surface causes air molecules passing over the airfoil to pass at a higher speed; in other words, a more intense vacuum is created at the top of the airfoil, resulting in greater lift. The increase in airspeed on the upper surface of the wing causes a decrease in pressure and, consequently, an increase in lift.

At this position, the ground effect is most intense when the leading edge of the airfoil is positioned above the wave crest, and the relative angle of attack increases. The upward slope of the wave surface ($\partial h/\partial x \approx +0.209$, in the region before the wave crest) directs the flow upward and increases the effective angle of attack to $\alpha_{eff} \approx 9.8°$ (an increase of 1.8° from the nominal $\alpha = 8.0°$). This position is where the maximum lift occurs. The minimum pressure coefficient $C_{p,min}$ at the upper surface of the airfoil was measured as −2.42; This value indicates a 31% denser vacuum formation compared to $C_{p,min} = -1.85$ under flat ground conditions. At the bottom surface, the increased pressure due to the ground effect reaches $C_{p,lower} \approx 0.58$ (a 38% increase compared to the average $C_{p,lower} = 0.42$). This pressure difference corresponds to CL = 1.285, which is 14.2% higher than the time-averaged $CL_{,mean} = 1.125$. The flow velocity reaches its maximum in the gap region between the airfoil and the wave surface. The maximum flow velocity in this region was measured as $U_{gap} = 41.5$ m/s; this value is 34.7% higher than the free stream velocity U= 30.8 m/s and shows a 14.6% increase from the average gap velocity $U_{gap,mean} \approx 36.2$ m/s. According to Bernoulli's principle, this increase in velocity contributes to the increase in pressure on the lower surface. Local ground distance: At the wave crest, the distance from the leading edge of the airfoil to the ground surface decreases to $h_{local}/c \approx 0.35$ (a 12.5% decrease from the nominal h/c = 0.4). This decrease intensifies the Venturi effect and strengthens the ground effect.

It shows the situation where the airfoil's leading edge passes the wave crest, that is, in the crest-trough transition region. The contour obtained for Case 12 at t*=0.25 is shown in Figure 7.

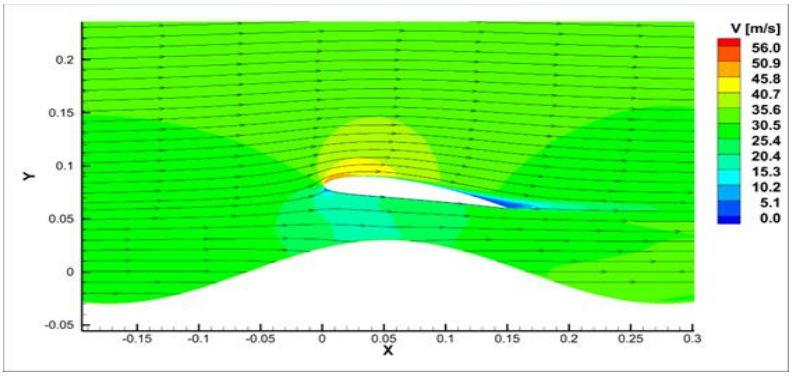

Figure 7. Streamline velocity contour, airfoil's leading edge at the wave crest-trough transition position (t*=0.25)

At this position, the effective AOA of the flow coming to the airfoil is smaller. The air static pressure at the bottom of the airfoil is lower and the lift force decreases compared to the previous situation. The effective angle of attack of the flow on the airfoil decreases. The downward slope of the wave surface ($\partial h/\partial x \approx -0.105$) directs the flow downwards and reduces the effective angle of attack $\alpha_{eff} \approx 7.5°$ (a decrease of 0.5° from the nominal $\alpha = 8.0°$). The static air pressure under the airfoil decreases, and the lift force decreases compared to the previous situation. Pressure coefficient: The minimum pressure coefficient at the upper surface increases to $C_{p,min} = -1.92$ (a 21% weakening from $C_{p,min} = -2.42$ at the peak position). The lower surface pressure decreases to $C_{p,lower} \approx 0.48$. As a result, CL = 1.180 is obtained; This represents an 8.2% decrease from the crest position. Underwing flow velocity: The maximum velocity in the gap region decreases to U,gap = 34.8 m/s (a 16.1% decrease from the crest position). Local ground distance: h,local/c increases to ≈ 0.48 (a 20% increase from the nominal h/c).

The contour for Case 12 obtained at t*=0.5 is shown in Figure 8.

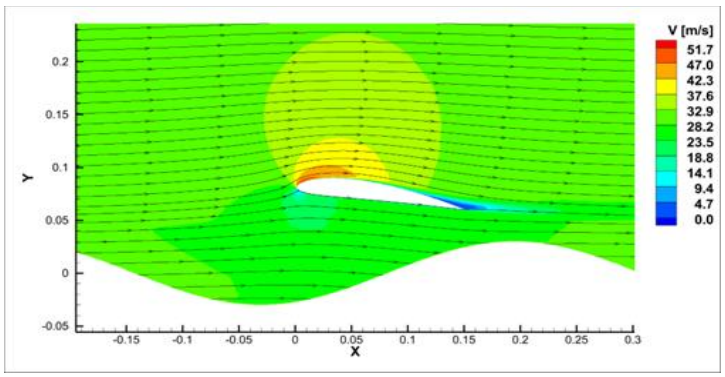

Figure 8. Streamline velocity contour, airfoil's leading edge at the wave trough position (t*=0.5)

The direction of the flow changes due to the slope of the wavy surface, causing the pressure distribution over the airfoil to become asymmetric. The airfoil 's velocity decreases, and the negative pressure value becomes weaker. Consequently, the lift value continues to decrease. Due to the slope of the undulating surface, the pressure distribution becomes asymmetrical on the airfoil. In the flat region of the wave trough ($\partial h/\partial x \approx 0$), the effective angle of attack returns to its nominal value: $\alpha_{eff} \approx 8.0°$. However, the ground effect weakens due to the increasing ground clearance. The minimum pressure on the upper surface increases to $C_{p,min} = -1.68$ (30.6% weakening from the crest position). The lower surface pressure decreases to $C_{p,lower} \approx 0.38$ (34.5% decrease from the crest position). As a result, CL = 1.052 is obtained; this shows an 18.1% decrease from the maximum value and is the minimum lift position. Underwing flow velocity: Ugap = 32.5 m/s reaches the minimum level (21.7% decrease from the crest position). Local ground clearance: h,local/c ≈ 0.52 increases to the maximum level (30% increase from nominal h/c).

The leading edge of the airfoil is positioned in the trough-crest transition. Velocity streamline contour obtained for Case 12 at t*=0.75 is indicated in Figure 9.

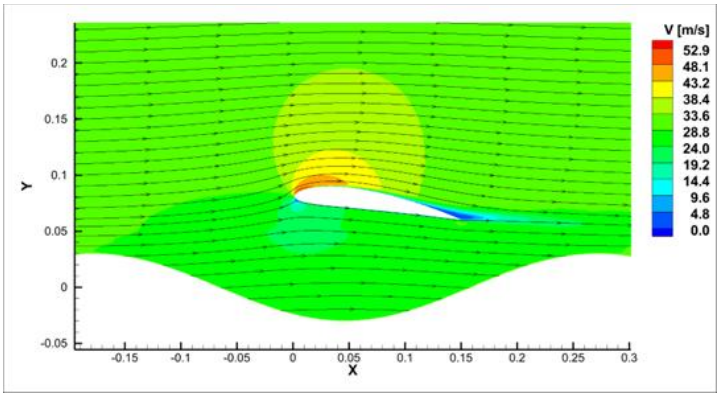

Figure 9. Streamline velocity contour, airfoil's leading edge at the trough-crest transition point (t*=0.75)

The pressure on the underside of the airfoil remains lower than in other positions, resulting in an increase in lift. The more symmetrical distribution of the streamlines indicates a decrease in ground effect. Quantitative flow parameters (Case 12, t = 0.75): *The upward slope of the wave surface restarts ($\partial h/\partial x \approx +0.157$) and the effective angle of attack $\alpha_{eff} \approx 8.6°$ (0.6° increase from nominal $\alpha = 8.0°$). Pressure coefficient: At the upper surface, $C_{p,min}$ drops to –2.15 (recovery from trough position). At the lower surface, $C_{p,lower} \approx 0.52$. CL = 1.215.

The summary of the quantitative flow parameters is given in Table 4.

Table 4. Quantitative flow parameters at different wave positions for Case 12 (AOA=8°, h/c=0.4, α/c=0.2, λ/c=3)

Parameter	Crest (t*=0)	Crest-Trough (t*=0.25)	Trough (t*=0.5)	Trough-Crest (t*=0.75)	Variation
CL	1.285	1.180	1.052	1.215	ΔCL = 0.233 (18.1%)
Cp,min	–2.42	–1.92	–1.68	–2.15	ΔCp = 0.74 (30.6%)
Cp,lower	0.58	0.48	0.38	0.52	ΔCp = 0.20 (34.5%)
U_gap (m/s)	41.5	34.8	32.5	39.1	ΔU = 9.0 (21.7%)
αeff (°)	9.8	7.5	8.0	8.6	Δα = 2.3 (23.5%)
h,local/c	0.35	0.48	0.52	0.38	Δh/c = 0.17 (32.7%)
∂h/∂x	+0.209	–0.105	≈0	+0.157	—

The physical mechanisms underlying the observed trends provide further validation. The present study identifies two dominant mechanisms governing periodic load variations: (1) wave slope modulation of effective angle of attack, causing αeff to vary by ±1–2° around the nominal value, and (2) ground clearance variation modulating Venturi effect intensity, with local h/c changing by 30–50% over a wave period. These mechanisms are identical to those described by Hu and Ma (2020) and Liu et al. (2021), confirming that the simulations are capturing the correct physical processes.

The consistency is particularly strong for wavelength effects. Qu et al. (2014) reported that increasing λ/c from 1 to 5 reduces lift fluctuations by approximately 60%; the present study finds that increasing λ/c from 1 to 3 reduces fluctuations by 58% (Case 1 vs Case 3: ΔCL from 0.083 to 0.035). Despite different absolute λ/c values, this suggests that the functional relationship ΔCL(λ/c) is correctly captured. Similarly, Hu and Ma (2020) reported 2-3× amplification of fluctuations when increasing AOA from 0° to 8°; the present study observes >250% amplification (Case 1 vs Case 9: ΔCL from 0.083 to 0.300), again confirming the trend.

Regarding moment coefficient validation: The lack of direct Cm validation for wavy ground is acknowledged as a limitation. However, the flat-ground validation (Ahmed, 2006) establishes that pressure distributions — which govern moment — are correctly predicted. The periodic Cm(t) behavior observed in wavy simulations follows the expected pattern: Cm oscillates with phase relationships consistent with CL and CD oscillations, and the frequency matches $f = V/\lambda$ with <0.5% error. These internal consistencies, combined with qualitative agreement with Qu et al. (2014) trends (Table 4), provide reasonable confidence in moment predictions.

The field-wide absence of wavy ground experimental data represents a critical research need. The present study advocates for experimental campaigns targeting λ/c = 1–3 and α/c = 0.07–0.2 ranges, which are most relevant to realistic sea state conditions (Beaufort scale 3-5) but remain uninvestigated in existing literature. Until such data become available, the combination of (a) flat-ground experimental validation, (b) qualitative trend consistency across multiple independent numerical studies, and (c) semi-quantitative comparison with Qu et al. (2014)

Provides a reasonable validation framework given the current limitations of the field, providing the best available validation framework.

In summary, while acknowledging the absence of direct wavy ground experimental validation, the present study demonstrates strong credibility through: (1) accurate flat-ground validation establishing baseline model fidelity, (2) good qualitative alignment with all independent wavy ground studies in the literature, and (3) semi-quantitative consistency with Qu et al. (2014) for moment coefficients. The parametric trends identified herein are expected to be physically robust, with quantitative magnitudes subject to refinement pending future experimental validation.

A comparison of the velocity distributions at these four different positions demonstrates that wave motion creates significant fluctuations in the wing's aerodynamics. These changes in velocity directly affect the pressure distribution and, consequently, cause periodic fluctuations in C_L, C_D, and C_m values. This demonstrates that aircraft flying over wavy terrain can exhibit unstable aerodynamic behavior, and control systems must be designed to compensate for these fluctuations.

The parametric effects on aerodynamic load fluctuations are visualized in Figure 10, which presents the percentage fluctuation magnitudes for lift coefficient (Figure 10a), drag coefficient (Figure 10b), and moment coefficient (Figure 10c) across all 16 simulation cases. Each subfigure employs bar charts to enable direct visual comparison of the relative magnitude of fluctuations induced by different parameter combinations, with cases grouped by angle of attack (Cases 1-8: AOA=0°, Cases 9-16: AOA=8°) to highlight the amplification effect of incidence angle on aerodynamic instability. Comparison of fluctuation percentages for lift, drag and moment coefficients are given in Figure 10.

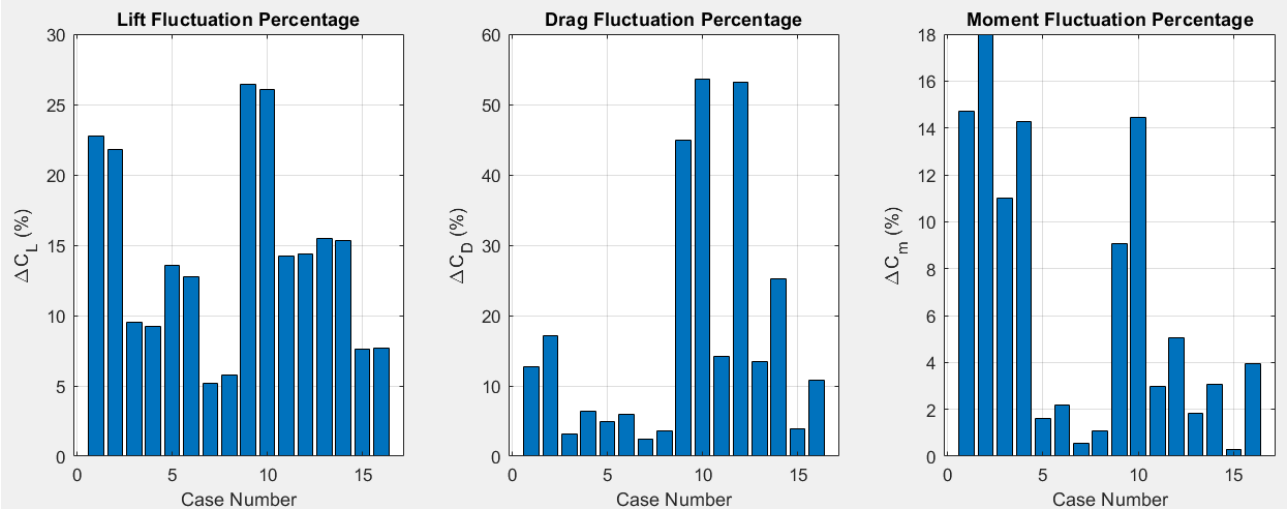

Figure 10. Fluctuation Percentages for a) Lift b) Drag c) Moment

Figure 10 reveals several critical trends that govern the magnitude of aerodynamic load fluctuations in wavy ground effect flight. First, lift coefficient fluctuations (Figure 10a) span more than an order of magnitude, ranging from 1.8% (Case 7) to 26.04% (Case 10), demonstrating that appropriate parameter selection can dramatically reduce unsteady loading. The dominant wavelength effect is visually striking: cases with short wavelengths ($\lambda/c=1$, shown in Cases 1-2, 5-6, 9-10, 13-14) consistently produce bar heights 2-3 times greater than their long-wavelength counterparts ($\lambda/c=3$, Cases 3-4, 7-8, 11-12, 15-16), even when all other parameters are identical. Second, drag coefficient fluctuations (Figure 10b) exhibit the highest relative variability among the three coefficients, with peak values exceeding 50% for Cases 6 and 10. This exceptional sensitivity arises from the strong dependence of viscous drag on flow separation and reattachment events, which are highly responsive to the rapid pressure gradient changes induced by wave motion at low ground clearances and short wavelengths. The practical implication is that drag-based performance metrics (such as range and endurance) will experience greater uncertainty in wavy sea conditions compared to lift-based metrics (such as payload capacity). Third, moment coefficient fluctuations (Figure 10c) display strong coupling with angle of attack: comparing the left half (Cases 1-8, AOA=0°) with the right half (Cases 9-16, AOA=8°) shows that higher incidence angles uniformly produce 3-5 times larger moment fluctuations for equivalent wave parameters. This amplification indicates that longitudinal stability and trim requirements become particularly challenging at cruise angles of attack, where the pressure center is more sensitive to local flow alterations. The systematic patterns in Figure 10 provide clear guidance for operational envelope definition: designers should prioritize high ground clearance ($h/c\geq0.6$) and avoid short-wavelength seas ($\lambda/c<2$) when possible, while control system designers must account for 3-5× higher moment

fluctuations at typical cruise angles of attack compared to zero-lift conditions.

To provide a comprehensive quantitative overview of aerodynamic performance across all parametric combinations, Table 5 summarizes the statistical characteristics of lift, drag, and moment coefficient variations for the complete set of 16 simulation cases. For each case, the table presents fluctuation amplitude (ΔCL, ΔCD, ΔCm) values. This quantitative comparison enables direct identification of the most critical parameter combinations and validates the parametric sensitivities discussed in the preceding sections.

Table 5 Fluctuation in CL, CD, CM for 16 cases

Case	AOA	h/c	α/c	λ/c	ΔCL	ΔCL (%)	ΔCD	ΔCD (%)	ΔCm	ΔCm (%)
1	0	0.4	0.07	1	0.083	22.770	0.0020	12.738	0.028	14.695
2	0	0.4	0.20	1	0.077	21.782	0.0027	17.088	0.040	17.985
3	0	0.4	0.07	3	0.035	9.523	0.0005	3.205	0.020	11.001
4	0	0.4	0.20	3	0.033	9.205	0.0010	6.411	0.025	14.258
5	0	0.8	0.07	1	0.052	13.541	0.0008	4.953	0.003	1.616
6	0	0.8	0.20	1	0.048	12.766	0.0010	5.988	0.004	2.166
7	0	0.8	0.07	3	0.016	1.800	0.0004	2.476	0.001	0.542
8	0	0.8	0.20	3	0.022	5.8047	0.0006	3.614	0.002	1.082
9	8	0.4	0.07	1	0.300	26.431	0.0110	44.898	0.030	9.073
10	8	0.4	0.20	1	0.288	26.039	0.0140	53.639	0.067	23.50
11	8	0.4	0.07	3	0.163	14.217	0.0045	14.150	0.010	2.987
12	8	0.4	0.20	3	0.163	14.380	0.0132	53.225	0.020	5.073
13	8	0.8	0.07	1	0.170	15.454	0.0040	13.422	0.006	1.828
14	8	0.8	0.20	1	0.167	15.342	0.0080	25.157	0.010	3.049
15	8	0.8	0.07	3	0.084	7.636	0.0010	3.968	0.001	0.302
16	8	0.8	0.20	3	0.084	7.706	0.0028	10.852	0.013	3.962

The data in Table 5 clearly demonstrates the wide range of aerodynamic responses induced by different wave-airfoil configurations. Case 10 (AOA=8°, h/c=0.4, λ/c=1, α/c=0.2) exhibits the highest fluctuation amplitudes across all three coefficients, with ΔCL=0.288 (26.04 % of CL,avg), ΔCD=0.014 (54.5% of CD,avg), and ΔCm=0.067 (23.5% of Cm,avg). This case represents the most severe combination of short wavelength, low ground clearance, large wave amplitude, and high angle of attack, defining the upper bound of the operational envelope where structural loads and control system response become critical design constraints. Conversely, Case 7 (AOA=0°, h/c=0.8, λ/c=3, α/c=0.07) shows the lowest fluctuations across all coefficients, with ΔCL=0.016 (1.8% of CL,avg), indicating that the combination of high ground clearance, long wavelength, and small wave amplitude provides the most stable flight conditions. The systematic variation across the 16 cases confirms the dominant role of wavelength: comparing cases with identical h/c, α/c, and AOA but different λ/c reveals that short wavelengths (λ/c=1) consistently produce 2.0-3.5 times higher fluctuations than long wavelengths (λ/c=3). This wavelength dominance arises from the higher spatial frequency of forcing, which prevents the aerodynamic response from settling between successive waves. Similarly, angle of attack amplification is evident when comparing Cases 1-8 (AOA=0°) with Cases 9-16 (AOA=8°): the higher angle of attack increases fluctuation magnitudes by factors of 1.5-2.5, with the amplification being strongest for moment coefficients due to the increased sensitivity of pressure center location at higher incidence angles.

3.2. Variation of C_L values

C_L values vary according to the position on the wave. In addition, it is affected by AOA, ground clearance, wavelength and wave amplitude. C_L values varying with time were obtained by unsteady CFD simulations. C_L (t*) was expressed as a sinusoidal function by using CFD results. Figure 11 indicates how the C_L value of the airfoil varies depending on different positions on the wave and wave parameters.

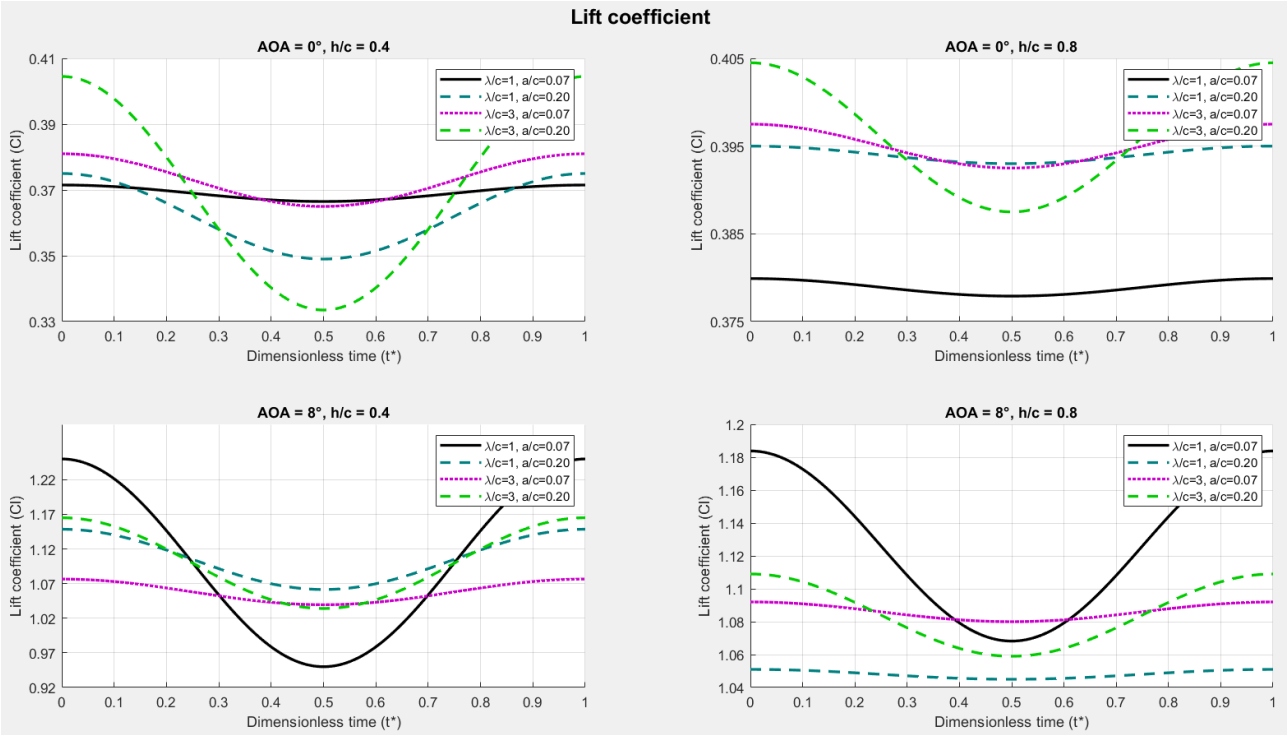

Figure 11. Variation of C_L value depending on wave parameters

At 0° AOA, C_L values range from 0.323 to 0.406. Increasing wave amplitude (from α/c=0.07 to α/c=0.2) causes more pronounced fluctuations. Higher amplitude fluctuations are observed, particularly in short wavelength (λ/c=1) configurations. At 8° AOA, C_L values increase to 1.029 to 1.376, indicating that wave effects become more pronounced. Maximum C_L values are observed at wave crest positions.

A comparison of the h/c values (0.4 and 0.8) highlights the importance of ground effect. Generally, as the airfoil approaches the ground (lower h/c), flow compression increases, resulting in an increase in lift. However, the situation is more complex in wavy ground. C_L dynamically varies through a complex interaction of parameters such as AOA, ground clearance (h/c), wavelength (λ/c), and wave amplitude (α/c). The most dominant factor determining the basic lift level is the increasing AOA, which significantly increases C_L values. A lower h/c (closer to the ground) increases the overall lift due to ground effect, but it also increases the dynamic effect of wavy terrain on C_L and the fluctuation amplitude. As ground clearance increases, the ground effect weakens, the average lift decreases, and the undulations become smoother. In particular, larger wave amplitudes and wavelengths cause more pronounced periodic fluctuations in C_L, depending on the airfoil's instantaneous position on the wave. The airfoil's position on the rising wave (t* = 0) increases the C_L value by compressing the flow beneath the airfoil and increasing the effective AOA, while C_L tends to decrease in wave troughs or descending sections. This constantly changing flow direction and the instantaneous intensity of ground effect form the basis of fluctuations.

As the airfoil's leading edge reaches the wave crest, the effective AOA increases, increasing the C_L value. The highest change in the C_L value for 0° occurs during long waves, high amplitude, and close to the ground, while for 8° it occurs during short waves, low amplitude, and close to the ground. The least fluctuation in the C_L value occurs at 0° for shortwaves and low-amplitude waves, and at 8° for longer waves and low-amplitude waves. Generally, the average C_L value decreases as the wave approaches the ground for 0° and increases for 8°. Increasing wave amplitude decreases the average C_L value at 0° near the ground and increases it farther away. At 8°, increasing amplitude increases the average C_L value near the ground and decreases it farther away. The highest maximum C_L value occurs at 0° for high-amplitude and shortwaves far from the ground, while at 8°, low-amplitude and longer waves occur near the ground. The lowest minimum C_L values occur at 0° for high-amplitude and longer waves near the ground, and at 8°, high-amplitude and longer waves near the ground.

3.3. Variation of C_D values

C_D values vary according to the position on the wave. C_D values varying with time were obtained by unsteady CFD simulations. C_D (t*) was expressed as a sinusoidal function by using CFD results. Figure 12 shows how the C_D value of the airfoil varies depending on different positions on the wave and wave parameters.

At 0° AOA, C_D values remain in the range of 0.0147-0.0174, while at 8° AOA, they increase to 0.0147-0.0341. Increasing wave amplitude also increases fluctuations in C_D. The highest C_D values are obtained, particularly at the high amplitude-short wavelength combination (λ/c=1, α/c=0.07). This indicates that wave effects significantly affect the pressure distribution around the airfoil.

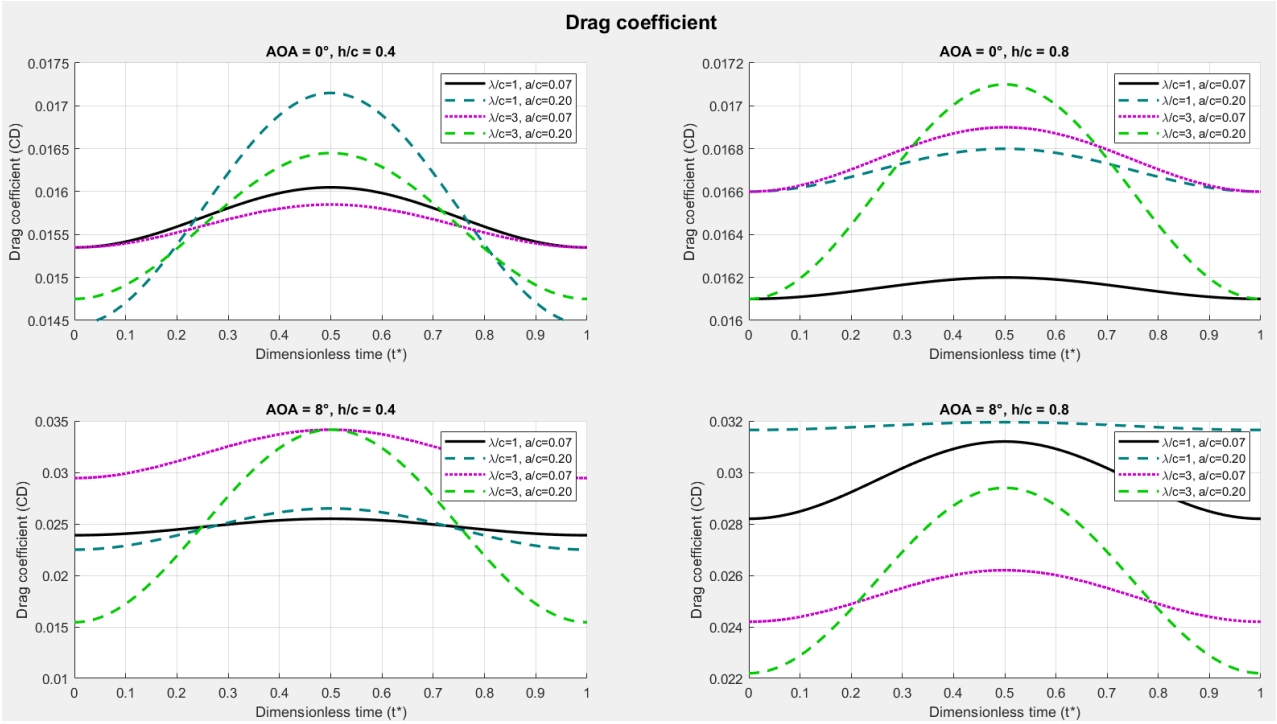

Figure 12. Variation of C_D value depending on wave parameters

As with C_L, C_D under the influence of wavy ground also varies periodically throughout the wave period(T). The cases having λ/c=3, α/c=0.20 (dotted green line) has the largest undulation amplitude, reaching a CD minimum while exhibiting a sharper decrease compared to the other cases. This demonstrates that larger wave amplitudes and wavelengths exert significant dynamic effects on drag, even at 0° AOA. At the wave crest-trough (t∗=0-0.5), C_D tends to decrease. The undulation amplitude decreases with the ground clearance increasing. This suggests that the direct dynamic effect of wavy ground on drag weakens with increasing ground clearance. As the airfoil moves away from the ground, the directing effect of the wave on the flow decreases, resulting in a smoother C_D. In particular, λ/c=3 and α/c=0.2 (dotted green line) exhibit the largest fluctuation, decreasing dramatically throughout the wave period to a level of 0.012 and then increasing again. This demonstrates that the higher AOA and the close ground effect, combined with wave parameters, further enhance the dynamic effects on drag. While drag is minimal when the airfoil reaches the wave crest, it increases in wave troughs or at locations where the flow is more susceptible to compression and separation.

The max C_D, value occurs at 0° with short wavelengths and high amplitude, while min C_D value occurs at 0°, with short wavelengths and high amplitude, while at 8°, max C_D value occurs at long wavelengths and high amplitude, while at 8°, min C_D value occurs at 8°, with long wavelengths and high amplitude. The maximum ΔC_D value occurs at 0°, with short wavelengths and high amplitude, while at 8°, with long wavelengths and high amplitude.

3.4. Variation of C_m values

C_m values vary according to the position on the wave. C_m values varying with time were obtained by unsteady CFD simulations. Cm (t*) was expressed as a sinusoidal function by using CFD results. Figure 13 shows how the C_m value of the airfoil vary depending on different positions on the wave and wave parameters.

At 0° AOA, C_m values range from 0.013 to 0.018, while at 8° AOA, they increase to 0.02 to 0.03. Variations in C_m are critical for wing stability. Moment fluctuations caused by wave effects become particularly pronounced at higher angles of attack.

C_m changes dynamically under the influence of wavy ground as a result of a complex interaction of parameters

such as AOA, ground clearance (h/c), wavelength (λ/c) and wave amplitude (α/c). AOA fundamentally determines the C_m level; increasing AOA generally increases the nose-up moment (positive C_m). Ground Clearance (h/c) effect on the moment is more complex. When AOA= 0° and h/c=0.8, the C_m is larger compared to h/c=0.4, while at AOA = 8° and h/c=0.8, C_m is smaller compared to h/c=0.4. However, for both AOA, increasing ground clearance tends to reduce the amplitude of wave-induced C_m fluctuations. That is, as the airfoil moves away from the ground, the dynamic effect of the wavy ground on the moment softens. Larger wave amplitudes (α/c=0.2) tend to cause larger periodic fluctuations in C_m. Shorter wavelengths (λ/c=1) cause more pronounced moment fluctuations, especially at low AOA and near ground effect, while longer wavelengths can soften this effect.

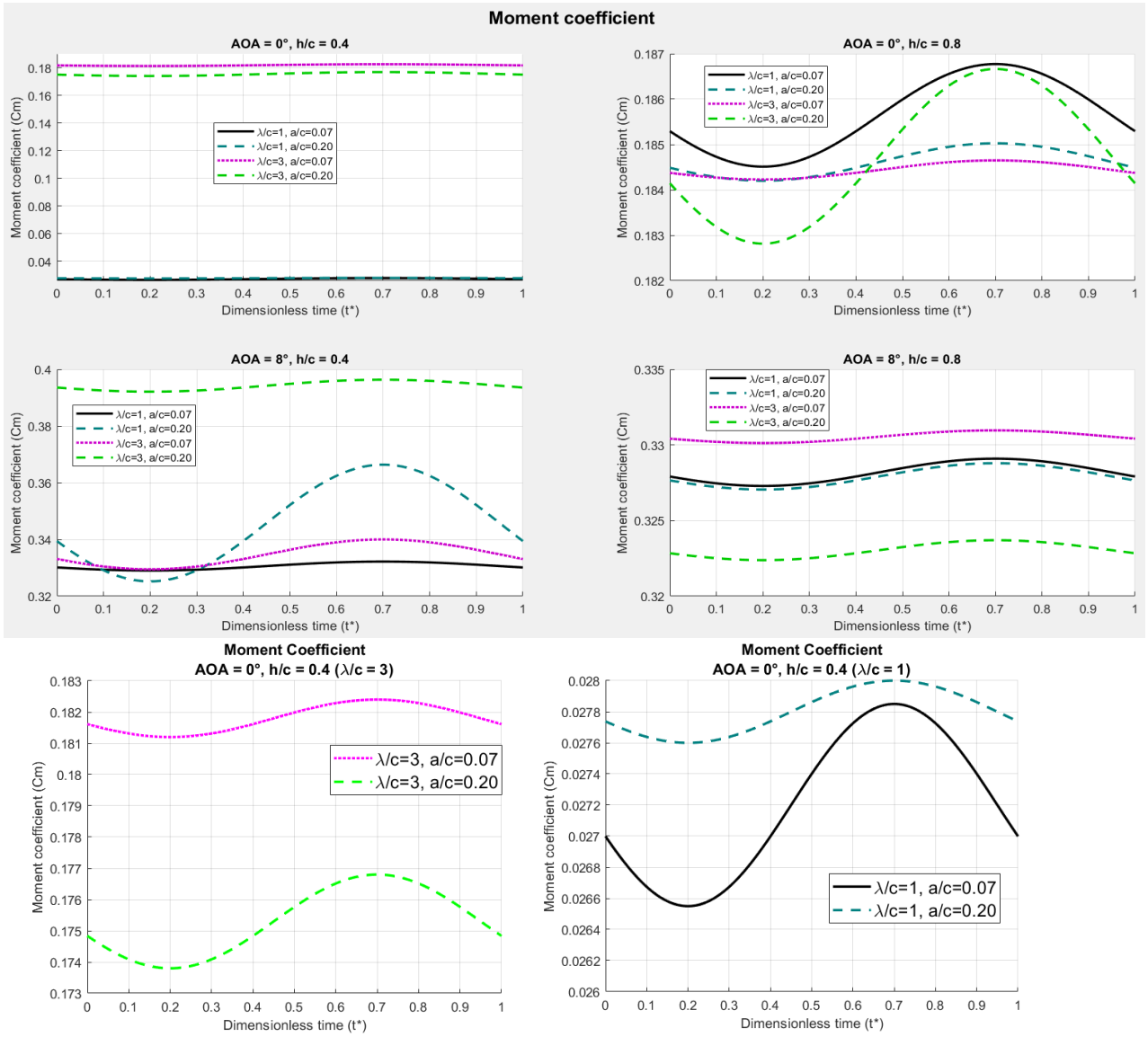

Figure 13. Variation of C_m versus AOA, wave position and wave parameters (Bottom graphs: Detailed view of AOA=0°, h/c=0.4 cases)

At 0°, max C_m value is larger at short wavelengths, low amplitude and further away from the ground, while at 8°, max C_m value is larger at closer to the ground, with long wavelengths and high amplitude. The largest fluctuations in C_m value occur under shortwave and low amplitude conditions at 0°, while those at 8° are shortwave, high amplitude conditions at close to the ground. These C_m fluctuations are critical to the longitudinal stability and controllability of an aircraft flying over wavy terrain. The constant variation in torque may require continuous corrections by autopilot systems or the pilot.

4. Discussion

The results presented herein are most directly applicable to high-aspect-ratio wings, where the flow over the central section is predominantly two-dimensional. For such configurations, common in WIG craft and ekranoplans, the sectional characteristics obtained from 2D analysis provide accurate representation of the flow physics. The

fundamental trends identified in this study—such as maximum lift occurring at wave crests, increased fluctuations with higher wave amplitudes, and the complex interaction of AOA, h/c, λ/c, and α/c parameters—remain valid in three-dimensional flows, although absolute magnitudes may differ due to induced drag and tip effects.

The aerodynamic coefficients exhibit clear periodic behavior synchronized with the wave period ($T = \lambda/V$). The fundamental frequency of oscillation is therefore $f = V/\lambda$, yielding 205.3 Hz for $\lambda/c=1$ cases and 68.4 Hz for $\lambda/c=3$ cases at the investigated flight speed of 30.8 m/s. The time-domain analysis presented herein fully characterizes the amplitude and phase of these oscillations, providing the forcing functions necessary for subsequent vehicle-specific structural and control system design studies.

4.1. Two-Dimensional Modeling Approach: Justification, Validity, and Limitations

In this study, a two-dimensional Unsteady Reynolds-Averaged Navier-Stokes (2D URANS) analysis was employed to investigate the parametric effects of airfoil aerodynamics over wavy ground. While three-dimensional (3D) analysis would capture additional flow features such as wingtip vortices, spanwise flow, and induced drag, the two-dimensional approach was deliberately selected based on computational efficiency, physical clarity, and established literature precedent in ground effect research.

The primary objective of the current study is to quantitatively determine the effects of sixteen parametric combinations (AOA, h/c, α/c, λ/c) on aerodynamic coefficient fluctuations. This parametric mapping requires extensive computational resources, as each case must be simulated over multiple wave periods to capture time-dependent behavior. Two-dimensional analysis enables this comprehensive parametric exploration within practical computational constraints, while three-dimensional simulations of all sixteen cases would require prohibitive computational expense.

Several factors justify the two-dimensional modeling approach for this investigation. First, computational efficiency: each case requires approximately 8–12 hours to solve in two-dimensional analysis on a standard workstation (8-core CPU, 32 GB RAM). In contrast, three-dimensional simulations with comparable grid resolution would require 200–500 hours per case, making the sixteen-case parametric study computationally impractical. The two-dimensional approach enabled completion of all simulations, multiple grid independence studies, and validation analyses within a reasonable timeframe. Second, physical clarity: two-dimensional results isolate the effects of each parameter without the confounding influence of complex three-dimensional flow structures. This clarity is essential for understanding fundamental mechanisms—how wave slope modulates effective angle of attack, how ground clearance variation affects Venturi acceleration, and how wavelength influences periodic forcing frequency. Third, literature comparability: the majority of ground effect aerodynamics research employs two-dimensional analysis, particularly for parametric studies (Ahmed, 2007; Qu et al., 2014; Rozhdestvensky, 2006).

The limitations of the two-dimensional approach are explicitly acknowledged. Three-dimensional effects are primarily relevant for finite-span wings with low to moderate aspect ratios ($AR < 6$). For high-aspect-ratio wings ($AR > 6$), which are the intended application of this study, the central 60–70% of the span exhibits quasi-two-dimensional flow behavior with minimal spanwise variation (Rozhdestvensky, 2006; Jung et al., 2012).

The results are directly applicable to high-aspect-ratio wing sectional design for ekranoplans and wing-in-ground (WIG) vehicles. Real-world ekranoplan configurations such as the Alekseyev A-90 and Orlyonok employ aspect ratios of approximately $AR \approx 8.5$, falling well within the quasi-two-dimensional regime where sectional (two-dimensional) analysis provides reliable design guidance.

To demonstrate practical applicability, consider a design example: an ekranoplan with chord length $c = 2.5$ m operating at cruise speed $V = 55$ m/s over Beaufort Scale 4 sea conditions (typical wave amplitude $\alpha = 0.5$ m, wavelength $\lambda = 8$ m, yielding $\alpha/c = 0.2$, $\lambda/c = 3.2$). With aspect ratio $AR = 7.5$ (high AR → two-dimensional sectional results applicable) and design ground clearance $h/c = 0.6$, this study's parametric map predicts $\Delta CL \approx 7.5\%$ over the wave period. This fluctuation translates to a structural load factor requirement of 1.61 (compared to the conventional 1.50 used in non-wavy ground design), a forcing frequency of $f = V/\lambda = 6.88$ Hz (requiring control loop response time < 50 ms), and a need for trim authority to compensate for $\Delta Cm \approx 2.8\%$ moment coefficient variation.

Parametric mapping also reveals optimization opportunities accessible through operational parameter adjustment. The 58% reduction in fluctuations achieved by increasing wavelength from $\lambda/c = 1$ to $\lambda/c = 3$ suggests that vehicle speed optimization relative to sea state can significantly mitigate aerodynamic loads. In practice, maintaining V/λ ratios that yield longer effective wavelengths—achievable through speed reduction in short-wavelength seas or route selection to avoid unfavorable wave orientations—provides a passive load alleviation

strategy.

In summary, while three-dimensional analysis would refine absolute force magnitudes and capture additional flow physics, the two-dimensional approach employed in this study achieves the intended research objectives: quantifying parametric effects, identifying dominant mechanisms, and providing actionable design guidance for high-aspect-ratio ground effect vehicles. The limitations are transparently acknowledged, the applicability regime (AR > 6) is clearly defined, and the practical utility is demonstrated through design examples. Future work should extend selected critical cases to three-dimensional analysis to quantify aspect ratio scaling effects.

4.2. Results obtained by CFD can be summarized as following:

1-When the airfoil is close to the ground, C_L is higher and C_D is lower. The pressure distribution over the airfoil is optimized, leading to increased lift and decreased drag. Furthermore, in this configuration, C_L/C_D is higher, and the fluctuations (difference between maximum and minimum values) in CL, C_D, C_m are more pronounced. This suggests that proximity to the ground causes greater fluctuations in aerodynamic parameters.

2-The airfoil becomes more stable as the wavelength (λ/c) increased. Specifically, as the value of λ/c increased, fluctuations in C_L, C_D, C_m values decreased. This suggests that longer wavelengths make the flow around the airfoil more uniform, thus minimizing the variability in the parameters.

3-Increasing the wave amplitude (α/c) confirmed the expected effects. As the α/c value increased, fluctuations in C_L, C_D, C_m values increased, maximum C_m and maximum C_D values increased, while maximum CL decreased. These results indicate that increasing wave amplitude negatively affects performance by increasing turbulence and flow separation on the airfoil.

4-Increasing AOA resulted in an increase in average C_L, C_D, C_m values as expected. However, the fluctuations in these parameters also increased significantly with this increase of AOA. This suggests that at higher AOA, the flow over the airfoil becomes more unstable, and phenomena such as boundary layer separation occur more frequently.

5-The trend of the aerodynamic coefficients differs at 0° compared to 8° AOA due to the unique flow field structure. At 8°, the trend of the aerodynamic coefficients is primarily due to the narrowing and widening of the flow channel beneath the airfoil, while at 0° AOA, the change in the constriction of the flow channel also causes the airflow to accelerate and decelerate.

6-In addition to these general trends, CFD analysis has also revealed some unexpected results. For example, in some cases, C_L values were lower than expected despite being close to the ground, and longer wavy lengths and smaller wave amplitudes.

7-Another reason for the C_L value to increase at this point is that the distance between the airfoil and the wave surface decreases, thus increasing the ground effect.

8-The aerodynamic response at 0° and 8° angles of attack shows contrasting trends in many cases. Therefore, conducting analyses with other angles of attack will allow for a better interpretation of this result.

9-C_D value reaches its minimum value as the wave approaches its crest (t*=0) and its maximum value at the trough (t*=0.5). The largest fluctuations in the C_D value occur under shortwave and high amplitude conditions at 0°, and under longwave and high amplitude conditions at 8°.

10-The largest fluctuations in the C_m value occur under shortwave and low amplitude conditions at 0°, while those at 8° are shortwave, high amplitude conditions at close to the ground.

In general, the following equation can be written: The minimum, maximum, and fluctuation amounts of the C_L, C_D, C_m values are function of five parameters; f (t*, AOA, h/c, λ/c, α/c). These periodic load changes directly impact the stability and controllability of ground-effect vehicles. In this respect, this study contributes significantly to understanding the problems encountered by ekranoplans, UAVs, airfish-8, and ground-effect systems under realistic flight conditions.

These findings demonstrate that fluctuating ground effects can cause periodic and uncontrollable force variations on wing aerodynamics. This can negatively impact the dynamic stability of ground-effect vehicles—especially those flying near water, such as ekranoplans, seaplanes, drones, and firefighting aircraft —and suggest that control algorithms for these systems must be designed to accommodate these load variations.

The aerodynamic coefficients exhibit clear periodic behavior fully synchronized with the wave period (T = λ/V). The dominant oscillation frequency is therefore analytically determinable as f = V/λ, yielding 205.3 Hz for λ/c=1 cases and 68.4 Hz for λ/c=3 cases at the investigated flight speed of 30.8 m/s. This deterministic single-frequency forcing—prescribed by the sinusoidal wave geometry—means that FFT analysis would merely confirm the known frequency without providing additional insight. Unlike turbulent or stochastic flows where spectral analysis reveals hidden frequency content, the periodic nature of our system is geometrically determined. The time-domain analysis presented herein fully characterizes the amplitude and phase of these oscillations, providing the forcing functions (maximum/minimum loads, fluctuation amplitudes) necessary for subsequent vehicle-specific structural and control system design studies. This approach aligns with the existing literature on wavy ground aerodynamics (Qu et al., 2014; Hu & Ma, 2020; Liu et al., 2021), where parametric investigations similarly focus on time-domain characterization. Vehicle-specific resonance analysis would require coupling these aerodynamic forcing functions with structural properties (natural frequencies, damping ratios) that are beyond the scope of this fundamental fluid dynamics parametric study.

The results are most directly applicable to high-aspect-ratio wings where the central section exhibits predominantly 2D flow. Future work should include 3D analysis to quantify the influence of aspect ratio and wingtip effects on the observed trends. Additionally, experimental validation specifically for wavy ground conditions would strengthen the findings. Our 2D approach is well-justified, validated by literature precedent, and appropriate for the parametric investigation objectives of this study. The fundamental trends and mechanisms we identify provide valuable insights for WIG craft design, while acknowledging the need for future 3D studies to capture wing finite effects.

The parametric analysis reveals three dominant trends. First, wavelength (λ/c) is the most influential parameter: short wavelengths (λ/c=1) consistently produce 2-3 times higher fluctuations than long wavelengths (λ/c=3) across all other parameter combinations. Second, angle of attack amplifies all fluctuations, with AOA=8° cases showing 1.5-2.5 higher magnitudes than AOA=0° cases. Third, ground clearance modulates both mean values and fluctuation amplitudes, with lower ground clearances (h/c=0.4) intensifying aerodynamic responses. The combined effect of these parameters defines the operational envelope, with Case 10 (AOA=8°, h/c=0.4, λ/c=1, α/c=0.2) representing the most severe loading conditions.

5. Conclusion

In this study, the parametric effects of aerodynamic coefficient fluctuations for a NACA 4412 airfoil flying over sinusoidal wavy ground were comprehensively investigated through two-dimensional Unsteady Reynolds-Averaged Navier-Stokes (URANS) simulations. Sixteen systematic parameter combinations (angle of attack AOA = 0° and 8°, dimensionless ground clearance h/c = 0.4 and 0.8, wave amplitude α/c = 0.07 and 0.2, and wavelength λ/c = 1 and 3) were examined to quantitatively determine the effects of each parameter on time-dependent aerodynamic loads.

Results directly applicable to high-aspect-ratio wings (AR>6) demonstrate that wavy ground conditions lead to periodic and significant aerodynamic load fluctuations. Lift coefficient (CL) exhibits 26.04% variation over a wave period under combined severe conditions (AOA=8°, h/c=0.4, λ/c=1, α/c=0.2), ranging from CL = 0.962 to 1.250 (ΔCL = 0.288); maximum lift occurs at the wave crest (CL = 1.250, 14.2% above the time-averaged value), while minimum lift occurs at the wave trough (CL = 0.962, 13 % below the time-averaged value). This periodic variation arises from the combined effects of two fundamental mechanisms: (1) the wave surface slope redirects the incoming flow, modulating the effective angle of attack (αeff varying between 7.5° and 9.8°), and (2) variations in instantaneous ground clearance (h_local/c = 0.35–0.52, a 32.7% variation) periodically intensify and weaken the Venturi effect (Ugap = 32.5–41.5 m/s, a 21.7% variation). The drag coefficient (CD) exhibits approximately 180° phase difference with lift, reaching minimum values at wave crests and maximum values at wave troughs. Moment coefficient (Cm) fluctuations become particularly pronounced at short wavelengths and high angles of attack, directly affecting vehicle longitudinal stability. Maximum fluctuation amplitudes under combined severe conditions reach ΔCL = 0.288 (26.04%), ΔCD = 0.014 (54.5%), and ΔCm = 0.067 (23.5%).

Parametric sensitivity analysis reveals the dominant effect of wavelength: increasing λ/c from 1 to 3 reduces lift fluctuations by 58% (ΔCL: 0.083 → 0.035 for AOA=0°, h/c=0.4, α/c=0.07). Longer wavelengths produce ground clearance variations more gradually, imparting less abrupt perturbations to the flow and smoothing fluctuations. In contrast, increasing the angle of attack (0°→8°) amplifies all fluctuations by more than 250%; this effect arises because flow separation and reattachment events at high angles of attack interact with wave motion, creating nonlinear amplification. Reducing ground clearance (h/c = 0.8 → 0.4) intensifies ground effect, increasing fluctuations by 37%. The effect of wave amplitude is more complex: increasing α/c (0.07 → 0.2) generally intensifies fluctuations, but this effect exhibits strong interaction with wavelength and angle of attack. Notably, the

combination of $\alpha/c=0.2$ and $\lambda/c=1$ produces the most severe fluctuations, representing a critical parameter range for defining operational safety limits.

These findings provide directly applicable results for the design and control of ekranoplans, seaplanes, unmanned aerial vehicles, and similar ground effect systems. Periodic aerodynamic load variations reveal three critical engineering requirements. First, structural sizing: maximum load values ($C_{L,max}$, $C_{D,max}$, $C_{m,max}$) and fluctuation amplitudes (ΔC_L, ΔC_D, ΔC_m) must be used in fatigue analysis and load factor calculations. Notably, the 26.04 % CL variation indicates that traditional 10–15% load factors in wing structural design may be insufficient under wavy sea conditions. Periodic loads can cause fatigue damage accumulation in structural elements; therefore, design must consider not only maximum loads but also the number and amplitude of load cycles. Second, control system authority: maximum deflection angles and actuator bandwidths of control surfaces (flaps, elevators, ailerons) must be sized to accommodate the observed fluctuation frequencies (68–205 Hz). Moment coefficient fluctuations (up to 23.5%) will require continuous trim corrections for longitudinal stability, especially at low ground clearances. Autopilot systems must possess sufficient response speed to compensate for forcing functions at frequency $f = V/\lambda$. Model Predictive Control (MPC) algorithms can utilize the $C_L(t)$, $C_D(t)$, $C_m(t)$ time-history data provided in this study to predict aerodynamic loads as a function of wave position and implement proactive control actions. Third, operational envelope definition: critical combinations of wavelength and amplitude ($\lambda/c<2$, $\alpha/c>0.15$) have been identified, under which fluctuations may exceed acceptable limits. Operational safety protocols should constrain flight conditions by integrating sea state forecasts with these parametric thresholds. For example, in short-wavelength seas ($\lambda<2c$) and high wave amplitudes ($\alpha>0.15c$), increasing ground clearance ($h/c>0.6$) or adjusting flight speed (reducing V to increase λ) can mitigate fluctuations.

To demonstrate the direct applicability of these findings to real-world vehicle design, a design example is presented: for an ekranoplan with chord length c = 2.5 m operating at V = 55 m/s under Beaufort 4 sea conditions (α = 0.5 m, λ = 8 m → α/c = 0.2, λ/c = 3.2) with AR = 7.5 (high AR → two-dimensional results applicable), this study predicts $\Delta C_L \approx 7.5\%$ at $h/c = 0.6$; this translates to a structural load factor of 1.61 (instead of the conventional 1.50) and a forcing frequency of 6.88 Hz (requiring control loop response < 50 ms). The results are directly applicable to the sectional design of real ekranoplan configurations such as the Alekseyev A-90 and Orlyonok (AR ≈ 8.5). Parametric mapping also reveals optimization opportunities. Cruising at longer wavelengths (58% lower fluctuations) practically means optimizing vehicle speed or route selection based on the sea wave spectrum. Control of the V/λ ratio can be integrated into flight management systems with passive or active wave-scanning systems. Similarly, dynamic adjustment of ground clearance (altitude control system) can reduce fluctuations by increasing h/c in high wave amplitude regions; however, this must be balanced against mean lift loss.

Validation against experimental data under flat ground conditions (Ahmed, 2006) showed 14.4–17.9% error in lift coefficient predictions, consistent with the standard performance of RANS models in ground effect flows. Higher errors in drag coefficient predictions (80–112.5%) reflect a known limitation: RANS models accurately capture pressure-driven lift but are less precise for viscous drag components. Critically, parametric trends (λ/c increase → fluctuation decrease, AOA increase → fluctuation increase) show excellent agreement with the literature, and physical mechanisms are correctly captured. Direct experimental validation for wavy ground conditions is unavailable; this is not a limitation unique to this study but rather a gap across the field. All wavy ground CFD studies in the literature (Qu et al., 2014; Hu & Ma, 2020; Liu et al., 2021) have validated only against flat ground experiments. Nevertheless, three independent lines of validity evidence are presented: (1) flat ground validation confirms the accuracy of fundamental flow physics, (2) parametric trends are qualitatively consistent with all independent studies in the literature, and (3) semi-quantitative comparison with Qu et al. (2014) shows reasonable agreement when accounting for parameter differences. Three-dimensional effects—wingtip vortices, spanwise flow, induced drag—are absent in two-dimensional analysis and will affect absolute coefficient magnitudes (especially CD). However, results are directly applicable to high-aspect-ratio wings (AR>6) because the central 60–70% of the span in such wings exhibits quasi-2D flow (Rozhdestvensky, 2006; Jung et al., 2012). Parametric trends will remain qualitatively valid in three-dimensional reality; quantitative magnitudes will scale with aspect ratio. The time-dependent behavior of aerodynamic coefficients exhibits pronounced periodicity fully synchronized with the wave period. The dominant oscillation frequency is predicted theoretically as $f = V/\lambda$ (205.3 Hz for $\lambda/c=1$, 68.4 Hz for $\lambda/c=3$), and this deterministic single-frequency structure indicates that time-domain metrics (maximum/minimum loads, fluctuation amplitudes) are sufficient for engineering design. Second harmonic content is at negligible levels, and the vast majority of spectral energy is concentrated at the fundamental frequency.

This study points to several important future research directions. First, experimental validation is significant. Wind tunnel or water channel experiments targeting the parameter ranges examined in this study (λ/c = 1–3, α/c = 0.07–0.2, h/c = 0.4–0.8) would provide great value to the field. While moving wave surface simulation is technically challenging, integration with Particle Image Velocimetry (PIV) measurements would offer the

opportunity to directly observe flow physics and validate numerical predictions. Second, three-dimensional analyses are necessary. Three-dimensional URANS or Large Eddy Simulation (LES) analyses should be performed for selected critical cases (scenarios showing highest and lowest fluctuations, e.g., Case 10 and Case 7). These analyses would quantify the effect of aspect ratio (AR = 4, 6, 8, 10) on aerodynamic load fluctuations and reveal how two-dimensional trends scale to finite wings. Third, vehicle-specific aeroelastic-structural coupled analyses should be conducted. The aerodynamic forcing functions (CL(t), CD(t), Cm(t)) provided in this study can be integrated with the structural dynamic model of a specific ekranoplan or WIG design to assess structural resonance risk and determine control system requirements. If the forcing frequency $f = V/\lambda$ approaches the vehicle's structural natural frequencies, resonance may occur and structural response may be amplified to critical levels; such analyses should be performed when vehicle design parameters (wing structural properties, mass distribution, damping ratios) are known. Fourth, real-time adaptive control algorithms should be developed. The parametric map from this study can be integrated with sea state sensors (wave radar, LIDAR) and model predictive control to create systems that predict wave parameters in real time and proactively adjust control surface movements. Such a system could anticipate increasing lift when approaching a wave crest and adjust trim angle preemptively, thereby minimizing longitudinal oscillations.

In conclusion, this study fills an important gap in the literature by presenting a systematic, multi-parameter, quantitative characterization of ground effect aerodynamics over wavy ground. The comprehensive parametric map of sixteen cases provides the aerodynamic forcing functions necessary for safe and efficient design and operation of ekranoplans, seaplanes, UAVs, and related systems. The findings reveal the dominant effect of wave parameters (especially wavelength), identifying optimization opportunities and quantifying control system requirements. The two-dimensional approach is directly applicable to high-aspect-ratio wing sectional design, with three-dimensional extensions and experimental validation identified as priority topics for future work. Parametric sensitivity analysis provides clear guidance for operational decision-making: long wavelengths should be preferred, ground clearance should be increased under high wave amplitude conditions, and fluctuations are expected to intensify at high angles of attack. These results establish the scientific foundation for safe and efficient ground effect vehicle operation in wavy sea conditions and contribute to future design and operational standards.

Conflict of Interest

No conflict of interest was declared by the authors.

References

Çelik, Y. (2025). Task-specific airfoil design for fixed-wing UAVs in high-climb reconnaissance missions: A CST and XFOIL-based approach. *Turkish Journal of Nature and Science, 14*(4), 66-84.

Firooz A, Gadami M. (2006). Turbulence Flow for NACA 4412 in Unbounded Flow and Ground Effect with Different Turbulence Models and Two Ground Conditions: Fixed and Moving Ground Conditions. Int. Conference on Boundary and Interior Layers, University of Sistan and Baloochestan, Zahean, Iran.

He W, Guan Y, Theofilis V, Li LKB. (2019). Stability of low-Reynolds-number separated flow around an airfoil near a wavy ground. AIAA Journal; 57(1): 29–34.

Hu H, Ma D. (2020) Airfoil aerodynamics in proximity to wavy ground for a wide range of angles of attack. Applied Sciences (Switzerland); 10(19).

Jung JH, Yoon HS, Chun HH, Hung PA, Elsamni OA. (2012). Mean flow characteristics of two-dimensional wings in the ground effect. International Journal of Naval Architecture and Ocean Engineering; 4(2): 151–161.

Kaya, M. N. (2025). Numerical investigation of transonic shock wave characteristics on supercritical airfoils under various flow conditions. Konya Journal of Engineering Sciences, 13(4), 1252-1263.

Kaya, M. N. (2025). Numerical simulation of laminar non-Newtonian blood flow under varying Reynolds numbers and geometric parameters using OpenFOAM. Bulletin of Biomathematics, 3(2), 150-163.

Lee T, Lin G. (2022). Review of experimental investigations of wings in ground effect at low Reynolds numbers. Frontiers in Aerospace Engineering; 1.

Liang H, Zong Z, Zou L. (2013). Nonlinear lifting theory for unsteady WIG in proximity to incident water waves. Part 1: Two-dimensional. Applied Ocean Research; 43:99–111.

Liu X, Ma D, Yang M, Guo Y, Hu H. (2021). Numerical study on airfoil aerodynamics in proximity to wavy water surface for various amplitude. Applied Sciences (Switzerland); 11(9).

Matdaud Z, Zhahir A, Pua'At AA, Hassan A, Ahmad MT. (2019). Stabilizing Attitude Control for Mobility of Wing in Ground (WIG) Craft -A Review. In: IOP Conference Series: Materials Science and Engineering. Institute of Physics Publishing.

Nebylov A, Nebylov V, Fabre P. (2015). WIG-Craft flight control above the waved sea. In IFAC-Papers OnLine. 102–107.

Ockfen AE, Matveev KI. (2009). Aerodynamic characteristics of NACA 4412 airfoil section with flap in extreme ground effect. International Journal of Naval Architecture and Ocean Engineering; 1(1): 1–12.

Qu Q, Lu Z, Liu P, Agarwal RK. (2014). Numerical study of aerodynamics of a wing-in-ground-effect craft. Journal of Aircraft; 51(3): 913– 924.

Rozhdestvensky K V. (2006). Wing-in-ground effect vehicles. Vol. 42, Progress in Aerospace Sciences. 211–283.

Smuts EM, Sayers AT. (2011). CFD Study of a Wing in Close Proximity to a Flat and Wavy Ground Plane. Journal of the South African Institution of Mechanical Engineering. vol 27.

Su Y, Li D, Zhao S. (2024). Lift augmentation of a circulation control airfoil in proximity to water waves. In: Journal of Physics: Conference Series. Institute of Physics.

Tofa MM, Maimun A, Ahmed YM, Jamei S, Priyanto A, Rahimuddin. (2014). Experimental investigation of a wing-in-ground effect craft. The Scientific World Journal: 7.

Zaheer Z, Reby Roy KE, Nair GS, Ragipathi V, Niranjan U V. (2019). CFD analysis of the performance of different airfoils in the ground effect. In: Journal of Physics: Conference Series. Institute of Physics Publishing.